Is shrub expansion into grasslands pushed or pulled? A spatial integral projection model for woody plant encroachment

Trevor Drees*[a,b], Brad M. Ochocki[b], Scott L. Collins[c], and Tom E.X. Miller[b]

[a]Department of Biology, Penn State University, State College, PA USA

[b]Program in Ecology and Evolutionary Biology, Department of BioSciences, Rice University, Houston, TX USA

[c]Department of Biology, University of New Mexico, Albuquerque, NM USA

July 25, 2022

*thd5066@psu.edu

Abstract

Encroachment[1] of shrubs into adjacent grasslands has become an increasingly reported phenomenon across the world, and such encroachment is either pulled forward by high population growth at the low-density encroachment front or pushed forward by higher-density areas behind the front. However, at sites such as Sevilleta National Wildlife Refuge in central New Mexico, little is known about whether encroachment is pushed or pulled, and the dynamics of encroachment are not well-understood. Here, long-term encroachment of creosotebush (Larrea tridentata), a native perennial shrub, stands in stark contrast with the stagnation in encroachment observed in recent decades. In order to better understand creosotebush encroachment at this site, we quantify it using a spatially structured population model where a wave of individuals travels at a speed governed by both dispersal and density-dependence. Results indicate that population growth rates generally increase with decreasing density, suggesting that encroachment is pulled by individuals at the low-density wave front, and the spatial population model predicts an encroachment rate of less than 2 cm per year. While the predicted rate of encroachment is consistent with observations over recent decades, it does not explain long-term creosotebush encroachment at the study site, suggesting that this process may occur in pulses when recruitment, seedling survival, or dispersal significantly exceed typical rates. Overall, our work demonstrates that individuals at low densities are likely the biggest contributors to creosotebush encroachment at this site, and that this encroachment is likely a process that occurs in large but infrequent bursts rather than at a steady pace.

[1] *I am not editing the abstract for now.*

Keywords

density-dependence, ecotones, woody encroachment, shrubs, integral projection model, grassland

Introduction

The recent and ongoing encroachment of shrubs and other woody plants into adjacent grasslands has caused significant vegetation changes across arid and semi-arid landscapes worldwide (Cabral et al., 2003; Gibbens et al., 2005; Goslee et al., 2003; Parizek et al., 2002; Roques et al., 2001; Trollope et al., 1989; Van Auken, 2009, 2000). The process of encroachment generally involves increases in the number or density of woody plants in both time and space (Van Auken, 2000), which can drive shifts in plant community structure and alter ecosystem processes (Knapp et al., 2008; Ravi et al., 2009; Schlesinger and Pilmanis, 1998; Schlesinger et al., 1990). Other effects of encroachment include changes in ecosystem services (Kelleway et al., 2017; Reed et al., 2015), declines in biodiversity (Brandt et al., 2013; Ratajczak et al., 2012; Sirami and Monadjem, 2012), and economic losses in areas where the proliferation of shrubs adversely affects grazing land and pastoral production (Mugasi et al., 2000; Oba et al., 2000).

Woody plant encroachment can be studied through the lens of spatial population biology as a wave of individuals that may expand across space and over time (Kot et al., 1996; Neubert and Caswell, 2000; Pan and Lin, 2012; Wang et al., 2002). Theory predicts that the speed of wave expansion depends on two processes: local demography and dispersal of propagules. First, local demographic processes include recruitment, survival, growth, and reproduction, which collectively determine the rate at which newly colonized locations increase in density and produce new propagules. Second, colonization events are driven by the spatial dispersal of propagules, which is commonly summarized as a probability distribution of dispersal distance, or "dispersal kernel". The speed at which expansion waves move is highly dependent upon the shape of the dispersal kernel, especially long-distance dispersal events in the tail of the distribution (Skarpaas

and Shea, 2007). Both demography and dispersal may depend on plant size, since larger plants often have improved demographic performance and release seeds from greater heights, leading to longer dispersal distances (Nathan et al., 2011). Accounting for population structure, including size structure, may therefore be important for understanding and predicting wave expansion dynamics (Neubert and Caswell, 2000).

Theory predicts that the nature of conspecific density dependence is another critical feature of expansion dynamics but this is rarely studied in the context of woody plant encroachment. Expansion waves typically correspond to gradients of conspecific density – high in the back and low at the front – and demographic rates may be sensitive to density due to intraspecific interactions like competition or facilitation. If the demographic effects of density are strictly negative due to competitive effects that increase with density then demographic performance is maximized as density goes to zero, at the leading edge of the wave. Under these conditions, the wave is "pulled" forward by individuals at the low-density vanguard (Kot et al., 1996), and targeting these individuals and locations would be the most effective way to slow down or prevent encroachment (cite?). However, woody encroachment systems often involve positive feedbacks whereby shrub establishment modifies the environment in ways that facilitate further shrub recruitment. For example, woody plants can modify their micro-climates in ways that elevate nighttime minimum temperatures, promoting conspecific recruitment and survival for freeze-sensitive species (D'Odorico et al., 2010; Huang et al., 2020). Positive density dependence (or Allee effects) causes demographic rates to be maximized at higher densities behind the leading edge, which "push" the expansion forward, leading to qualitatively different expansion dynamics (Keitt et al., 2001; Kot et al., 1996; Lewis and Kareiva, 1993; Sullivan et al., 2017; Taylor and Hastings, 2005; Veit and Lewis, 1996). Pushed expansion waves generally have different shapes (steeper density gradients) and slower speeds

than pulled waves (Gandhi et al., 2016), and may require different strategies for managing or decelerating expansion (check Taylor and Hastings ref). The potential for positive feedbacks is well documented in woody encroachment systems but it remains unclear whether and how strongly these feedbacks decelerate shrub expansion and influence strategies for management of woody encroachment.

In this study, we linked woody plant encroachment to ecological theory for invasion waves, with the goals of understanding how seed dispersal and density-dependent demography drive encroachment, and determining whether the encroachment wave is pushed or pulled. Throughout the aridlands of the southwestern United States, shrub encroachment into grasslands is well documented (D'Odorico et al., 2012) but little is known about the dispersal and demographic processes that govern it. Our work focused on encroachment of creosotebush (*Larrea tridentata*) in the northern Chihuahuan Desert. Expansion of this species into grasslands over the past 150 years has been well documented, leading to decreased cover of *Bouteloua eriopoda*, the dominant foundation species of Chihuahuan desert grassland (Buffington and Herbel, 1965; Gardner, 1951; Gibbens et al., 2005). As in many woody encroachment systems, creosotebush expansion generates ecotones marking a transition from dense shrubland to open grassland, with a transition zone in between where shrubs can often be found interspersed among grasses (Fig. 1).

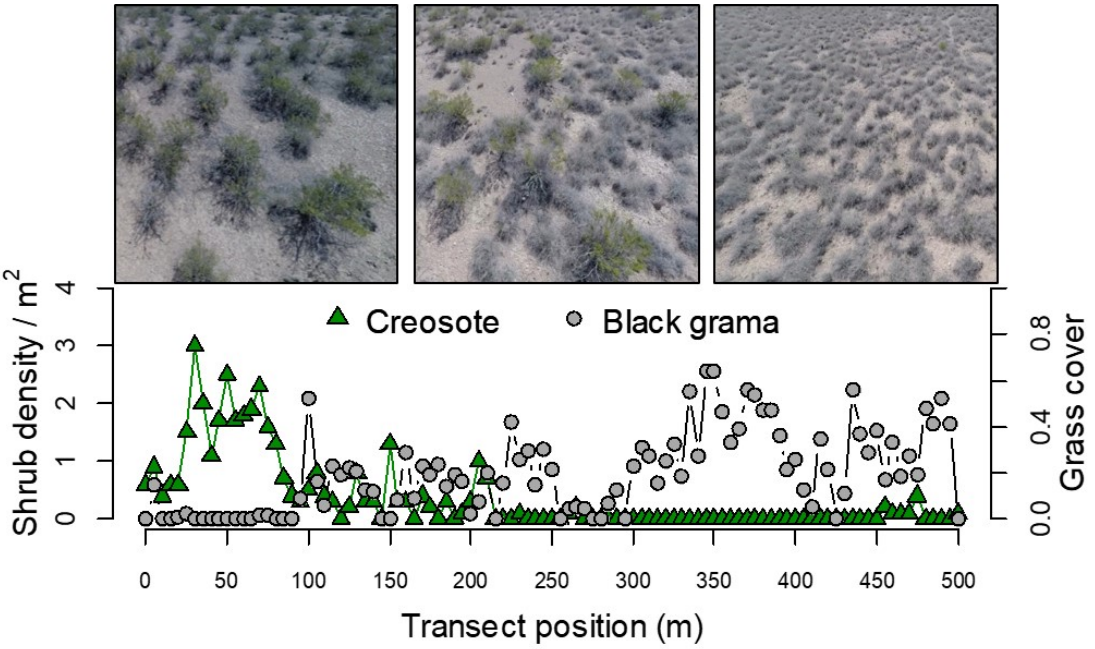

Figure 1: Example of an ecotone transect at Sevilleta LTER, spanning gradients of creosotebush and black grama grass. Photo credits: TEX Miller

Historically, creosotebush encroachment into grasslands is believed to have been driven by a combination of factors including overgrazing, drought, variability in rainfall, and suppression of fire regimes Moreno-de las Heras et al. (2016). These shrubs are also thought to further facilitate their own encroachment through positive feedbacks (D'Odorico et al., 2012; Grover and Musick, 1990) by modifying their environment in ways that favor continued growth and recruitment, including changes to the local microclimate (D'Odorico et al., 2010) and rates of soil erosion (Turnbull et al., 2010). Such positive feedback also involve suppression of herbaceous competitors, reducing competition as well as the amount of flammable biomass used to fuel the fires that keep creosotebush growth in check (Van Auken, 2000). We hypothesized that, given potential for positive

feedback mechanisms, the rarity of conspecifics at the low-density encroachment front may depress demographic performance and generate pushed-wave dynamics.

We used a combination of observational and experimental data from shrub ecotones in central New Mexico to parameterize a spatial integral projection model (SIPM) that predicts that speed of encroachment (m/yr) resulting from lower-level demographic and dispersal processes. Our data came from demographic surveys and experimental transplants along replicate ecotone transects spanning a gradient of shrub density, and seed drop experiments to estimate the properties of the dispersal kernel. We focused on wind dispersal of seeds, since little is known about the natural history of dispersal in this system and the seeds lack rewards to attract animal dispersers. We also used re-surveys of permanents transects as an independent measure of encroachment that provided a benchmark against which to evaluate model predictions. The SIPM accounts for size-structured demography of creosotebush, allows us to test whether shrub expansion is pulled by the low-density front or pushed from the high-density core, and identifies the local (demographic) and spatial (seed dispersal) life cycle transitions that most strongly contribute to expansion speed[2]. We address the following specific questions:

1. What is the nature of conspecific density dependence in demographic vital rates along shrub encroachment ecotones? Is encroachment pulled by the individuals at the front or pushed by individuals behind it?

2. What is the seed dispersal kernel for this species and how does this vary with maternal plant size?

3. What is the predicted rate of expansion from the SIPM and which lower-level processes most strongly affect the expansion speed?

[2] *we will need to stay consistent with the language of encroachment/expansion/invasion. For now I am swictihg a lot.*

4. How does the observed rate of encroachment in the recent past compare to model predictions?

Materials and methods

Study species

Creosotebush *Larrea tridentata* is a perennial, drought-resistant shrub that is native to the arid and semiarid regions of the southwestern United States and northern Mexico. High-density areas of creosotebush consist largely of barren soil between plants due to the "islands of fertility" these shrubs create around themselves (Reynolds et al., 1999; Schlesinger et al., 1996), though lower-density areas will often contain grasses in the inter-shrub spaces (Fig. 1). In our northern Chihuahuan desert study region creosotebush reproduces sexually, with numerous small yellow flowers giving rise to highly pubescent spherical fruits several millimetres in diameter; these fruits consist of five carpels, each of which contains a single seed. Seeds are dispersed from the parent plant by gravity and wind, with the possibility for seeds to subsequently be transported by animals or water (Maddox and Carlquist, 1985). In other regions, this species also reproduces asexually and can give rise to long-lived clonal stands (Vasek, 1980), but this does not occur in our study region. The foliage is dark green, resinous, and unpalatable to most grazing and browsing animals (Mabry et al., 1978).

Study site

We conducted our work at the Sevilleta National Wildlife Refuge (SNWR), a Long-Term Ecological Research (SEV-LTER) site in central New Mexico. The refuge exists at the intersection of several eco-regions, including the northern Chihuahuan Desert, Great Plains

grassland, and steppes of the Colorado Plateau. Annual precipitation is approximately 250 mm, with the majority falling during the summer monsoon season from June to September. The recruitment events that facilitate creosotebush expansion are thought to be highly episodic (Peters and Yao, 2012), and this may be linked to fluctuations in monsoon precipitation(Bowers et al., 2004; Boyd and Brum, 1983). Monsoon precipitation during the study years (2013-2017) was [summarise climate data].

Demographic data

Ecotone transects

We collected demographic data during early June of every year from 2013-2017. This work was conducted at four sites in the eastern part of SNWR[3] (one site was initiated in 2013 and the other three in 2014), with three transects at each site. All transects were situated along a shrubland-grassland ecotone so that a full range of shrub densities was captured: each transect spanned core shrub areas, grassland with no or few shrubs, and the transition between them. Lengths of these transects varied from 200 to 600 m, determined by the strength of vegetation transition since "steep" transitions required less length to capture the full range of shrub density.

We quantified shrub density in 5-meter "windows" along each transect, including all shrubs within one meter of the transect on either side (shrubs that partially overlapped with the census area were included). Densities were quantified once for each transect (in 2013 or 2014) and were assumed to remain constant for the duration of the study, a reasonable assumption for a species with very low recruitment and very high survival of established plants. Given the population's size structure, we weighted the density of each window by the sizes of the plants, which we quantified as volume (cm^3). Volume

[3] *would a map be helpful?*

was calculated as that of an elliptic cone: $V_i = \frac{\pi h}{3}\frac{lw}{4}$ where l, w, and h are the maximum length, maximum width, and height, respectively. Maximum length and width were measured so that they were always perpendicular to each other, and height was measured from the base of the woody stem at the soil surface to the tallest part of the shrub. The weighted density for a window was then expressed as log(volume) summed over all plants in the window.

Observational census

At approximately 50-m intervals along each transect we tagged up to 10 plants for annual demographic census and recorded their local (5-m resolution) window so that we could connect individual demographic performance to local density. These tagged shrubs were revisited every June and censused for survival (alive/dead), size (width, length, and height, as above), flowering status, and fertility of flowering plants (numbers of flowerbuds, flowers, and fruits). In instances where shrubs had large numbers of reproductive structures that would be difficult to reliably count (a large shrub may have thousands of flowers or fruits), we made counts on a fraction of the shrub and extrapolated to estimate whole-plant reproduction. Creosotebush does not have one discrete reproductive event per year; instead, flowering may occur throughout much of the warm season. By combining counts of buds, flowers, and fruits we intended to capture a majority of the season's reproductive output, assuming that all buds and flowers will eventually become fruits. Our measurements of reproductive output are therefore conservative and may underestimate total seed production for an entire transition year. Each year, we searched for new recruits within one m on either side of the transect. New recruits were tagged and added to the demographic census. The observational census included a total of 522 unique individuals.

Transplant experiment

We conducted a transplant experiment in 2015 to test how shrub density affects seedling survival. This approach complemented observational estimates of density dependence and filled in gaps for a part of the shrub life cycle that was rarely observed due to low recruitment. Seeds for the experiment were collected from plants in our study population in 2014. Seeds were germinated on Pro-Mix potting soil (Quakertown, PA) in Fall 2014 and seedlings were transferred to 3.8 cm-by-12.7 cm cylindrical containers and maintained in a greenhouse at Rice University. Seedlings were transported to SNWR and transplanted into the experiment during July 27-31, 2015. Transplant timing was intended to coincide with the monsoon season, when most natural recruitment occurs.

The transplant experiment was conducted at the same four sites and three transects per site as the observational demographic census, where we knew weight shrub densities at 5-m window resolution. We established 12 1-m by 1-m plots along each transect. Plots were intentionally placed to capture density variation: four plots were in windows with zero shrubs, four plots were placed in the top four highest-density windows on the transect, and the remaining four plots were randomly distributed among the remaining windows with weighted density greater than zero. Plots were placed in the middle of each 5-m window (at meter 2.5) and were divided into four 0.5-m by 0.5-m subplots. We divided each subplot into nine squares (0.125-m by 0.125-m) and recorded ground cover of each square as one of the following categories: bare ground, creosotebush, black grama (*B. eriopoda*), blue grama (*B. gracilis*), other grass, or "other". Each subplot received one transplanted shrub seedling, for a total of 48 transplants per transect, 144 transplants per site, and 576 transplants in the entire experiment. Each site was set up on a different day and there was a significant monsoon event after the third and before the fourth site. This resulted in differential mortality that appears to be related

to site (captured as a statistical random effect) but more likely reflects the timing of the monsoon event relative to planting (moist soil likely promoted transplant survival). We revisited the transplant experiment on October 24, 2015 to survey mortality. After that first visit, transplants were censused along with the naturally occurring plants each June, following the methods described above.

Demographic analysis

We fit statistical models to the demographic data and used AIC-based model selection to evaluate empirical support for alternative candidate models. The top statistical models were then used as the vital rate sub-models of the SIPM, so there is a strong connection between the statistical and population modeling, as is typical of integral projection modeling. Our analyses focused on the following demographic vital rates: survival, growth, probability of flowering, fertility (flower and fruit production), seedling recruitment, and seedling size. Most of these vital rates were modeled as a function of plant size, and all of them included the possibility of density dependence.

The alternative hypotheses of pushed versus pulled wave expansion rest on how the rate of population increase (λ), derived from the combination of all vital rates, respond to density. We were particularly interested in whether demographic performance was maximized as local density goes to zero (pulled) or at non-zero densities behind the wave front (pushed). To flexibly model density dependence and detect non-monotonic responses, we used generalized additive models in the R package 'mgcv' (Wood, 2017). For each vital rate, we fit candidate models with or without a smooth term for local weighted density (among other possible covariates). To avoid over-fitting, we set the 'gamma' argument of gam() to 1.8, which increases the complexity penalty, results in smoother fits (Wood, 2017), and makes our approach more conservative (other gamma

values yielded qualitatively similar results). We pooled data across transition years for analysis. All models included the random effect of transect (12 transects across 4 sites); we did not attempt to model both site and transect-within-site random effects due to the low numbers of each. All vital rate functions used the natural logarithm of volume (cm^3) as the size variable and the sum of log(volume) as the weighted density of a transect window.

Survival. We modeled survival or mortality in year $t+1$ as a Bernoulli random variable with three candidate models for survival probability. These included smooth terms for initial size in year t only (1), initial size and weighted density (2), and both smooth terms plus an interaction between initial size and weighted density (3). We analyzed survival of experimental transplants and observational census plants together in the same analyses, with a fixed effect of transplant status (yes/no) included in all candidate models. Since recruits and thus mortality events were both very rare in the observational survey, this approach allowed us to "borrow strength" over both data sets to generate a predictive function for size- and possibly density-dependent survival while statistically accounting for differences between experimental and naturally occurring plants. Because we had additional, finer-grained cover data for the transplant experiment that we did not have for the observational census, we conducted an additional stand-alone analysis of transplant survival that explored the influence of covariates at multiple spatial scales (Appendix).

Growth. We modeled size in year $t+1$ as a Gaussian random variable. There were nine candidate models for growth. The simplest model (1) defined the mean of size in year $t+1$ as a smooth function of size in year t and constant variance. Models (2) and (3) had constant variance but the mean included smooth terms for initial size and weighted density (2) or both smooth terms plus an interaction between initial size and weighted

density (3). Models 4-6 had the same mean structure as 1-3 but defined the standard deviation of size in year $t+1$ as a smooth function of initial size. Models 7-9 mirrored 4-6 and additionally included a smooth term for weighted density in the standard deviation. Modeling growth correctly is important because it defines the probability of any future size conditional on current size, a critical element of the IPM transition kernel. We verified that the AIC-selected model described the data well by simulating data from it and comparing the moments (mean, variance, skewness, and kurtosis) of simulated and real data.

Flowering and fruit production. We modeled shrub reproductive status (vegetative or flowering) in year t as a Bernoulli random variable with three candidate models for flowering probability. These included smooth terms for current size (in year t) only (1), size and weighted density (3), and both smooth terms plus an interaction between size and weighted density. We modeled the reproductive output of flowering plants (the sum of flowerbuds, open flowers, and fruits) in year t as a negative binomial random variable. There were three candidate models for mean reproductive output that corresponded to the same three candidates for flowering probability.

Recruitment and recruit size. We modeled seedling recruitment in each transect window as a binomial random variable given the number of total seeds produced in that window in the preceding year. There were two candidate models, with and without an influence of weighted density on the per-seed recruitment probability. To estimate window-level seed production, we used the best-fit models for flowering and fruit production and applied this to all plants in each window that we observed in our initial density surveys. We assume that recruits come from the previous year's seeds and not from a long-lived soil seed bank.

We modeled recruit size as a Gaussian-distributed random variable and fit four candidate models including an influence of weighted density on mean, variance, both, and neither.

Density-dependent IPM

The size- and density-dependent statistical models comprised the sub-models of a density dependent Integral Projection Model (IPM) that we used to evaluate how the shrub population growth rate responded to con-specific density; we present this non-spatial model before layering on the spatial dynamics generated by seed dispersal. A basic density-independent IPM predicts the number of individuals of size $x\prime$ at time $t+1$ ($n(x\prime, t+1)$) based on a demographic projection kernel (K_{dem}) that gives the rates of transition from sizes x to $x\prime$ from times t to $t+1$ and is integrated over the size distribution from the minimum (L) to maximum (U) sizes. In a density-dependent IPM, components of the projection kernel may respond to population abundance and structure:

$$n(x\prime, t+1) = \int_L^U K_{dem}(x\prime, x, \tilde{n}(t)) n(x,t)\, dx \tag{1}$$

Here, $\tilde{n}(t)$ is some function of population structure $n(x,t)$ such as the total density of conspecifics ($\tilde{n}(t) = \int n(x,t)\, dx$) or, as in our case, total density weighted by size ($\tilde{n}(t) = \int xn(x,t)\, dx$). For simplicity, in the analyses that follow we do not model density as a dynamic state variable; instead, we treat density as a static covariate ($\tilde{n}(t) = \tilde{n}$) and evaluate the IPM at a range of density values. As in our statistical modeling, the size variable of the IPM ($x, x\prime$) was $log(cm^3)$.

For our model, the size- and density-dependent demographic transitions captured by the projection kernel include growth or shrinkage (g) from size x to $x\prime$ conditioned on survival (s) at size x (combined growth-survival function $G(x\prime, x, \tilde{n}) = g(x\prime, x, \tilde{n})s(x, \tilde{n})$),

and the production of new size-$x\prime$ individuals from size-x parents ($Q(x\prime, x, \tilde{n})$). Reproduction reflects the probability of flowering at size x (p), the number of seeds produced by flowering plants (d), the per-seed probability of recruitment (r), and the size distribution of recruits (c). Collectively, the rate at which x-sized individuals produce $x\prime$-sized individuals at density $\tilde{n}$ is given by the combined reproduction-recruitment function $Q(x\prime, x, \tilde{n}) = p(x, \tilde{n})d(x, \tilde{n})r(\tilde{n})c(x\prime, \tilde{n})$. Thus, we can express the projection kernel as:

$$K_{dem}(x\prime, x, \tilde{n}) = G(x\prime, x, \tilde{n}) + Q(x\prime, x, \tilde{n}) \tag{2}$$

For analysis, we evaluated the IPM kernel over a range of local densities from the minimum to the maximum of weighted density values from the 5-meter windows ($0 \leq \tilde{n} \leq \tilde{n}_{max}$). At each density level, we discretized the IPM kernel into a 200×200 approximating matrix and calculated the asymptotic growth rate $\lambda(\tilde{n})$ as its leading eignevalue. We extended the lower (L) and upper (U) integration limits to avoid unintentional "eviction" using the floor-and-ceiling method (Williams et al., 2012).

We sought to characterize the shape of density dependence: whether fitness declined monotonically or not with increasing density. We quantified uncertainty in the density-dependent growth rate $\lambda(\tilde{n})$ by bootstrapping our data. For each bootstrap, we randomly sampled 75% of our demographic data, re-ran the statistical modeling and model selection, and used the top vital rate models to generate $\lambda(\tilde{n})$ for that data subset. We repeated this procedure for 500 bootstrap replicates.

Dispersal modelling

WALD dispersal model. Dispersal kernels were calculated using the WALD, or Wald analytical long-distance dispersal, model that uses a mechanistic approach to predict disper-

sal patterns of plant propagules by wind. The WALD model, which is based in fluid dynamics, can serve as a good approximation of empirically-determined dispersal kernels (Katul et al., 2005; Skarpaas and Shea, 2007) and may be used when direct observations of dispersal are not available. Under the assumptions that wind turbulence is low, wind flow is vertically homogenous, and terminal velocity is achieved immediately upon seed release, the WALD model simplifies a Lagrangian stochastic model to create a dispersal kernel that estimates the likelihood a propagule will travel a given distance (Katul et al., 2005). Our dispersal kernel takes the form of the inverse Gaussian distribution

$$p(r) = \left(\frac{\lambda'}{2\pi r^3}\right)^{\frac{1}{2}} \exp\left[-\frac{\lambda'(r-\mu')^2}{2\mu'^2 r}\right] \tag{3}$$

that is a slight adaptation[4] from equation 5b in Katul et al. (2005), using r to denote dispersal distance. Here, λ' is the location parameter and μ' is the scale parameter, which depend on environmental and plant-specific properties of the study system. (We use λ' for consistency with notation in related papers, but λ' the dispersal location parameter should not be confused with λ the geometric growth rate.) The location and scale parameters are defined as $\lambda' = (H/\sigma)^2$ and $\mu' = HU/F$; these are functions of the height H of seed release, wind speed U at seed release height, seed terminal velocity F, and the turbulent flow parameter σ that depends on both wind speed and local vegetation roughness. We parameterized the WALD dispersal kernel using windspeed data from the SEV-LTER weather station nearest our study site (Moore and Hall, 2022) and seed terminal velocity data from laboratory-based seed-drop experiments (Appendix A). We integrated the dispersal kernel over observed variation in wind speeds, seed terminal velocity, and release height within the height of a shrub. Therefore the dispersal kernel for a shrub of height U was given by:

[4] *unclear what this refers to*

$$K_{disp} = \iiint p(F)p(U)p(z)p(r)\,dF\,dU\,dz \tag{4}$$

and $p(F)$ and $p(U)$ are the PDFs of the terminal velocity F and wind speed U, respectively, and $p(z)$ is the uniform distribution from the minimum seed release height ($0.15m$, the height at which grass cover interferes with wind dispersal) to H. Methods for our seed data collection and technical details of dispersal kernel modeling are provided in Appendix A.

Spatial integral projection model

We used a spatial integral projection model to piece together seed dispersal and density-dependent demography, and generate predictions for the rate of shrub expansion that results from this combination of local and spatial processes. The spatially explicit model builds upon the non-spatial model (Eq. 1) and adds a spatial variable (z, z') such that demographic transitions occur across both time and space according to a combined demography-dispersal kernel $\tilde{K}$:

$$n(x\prime, z\prime, t+1) = \int_{-\infty}^{+\infty} \int_{L}^{U} \tilde{K}(x\prime, x, z\prime, z, \tilde{n}(z,t))n(x,z,t)\,dx\,dz \tag{5}$$

Here, $\tilde{K}(x\prime, x, z\prime, z, \tilde{n}(z,t))$ describes the transition from size x and location z to size $x\prime$ and location $z\prime$ given density $\tilde{n}(z,t)$ at starting location z. As before, $\tilde{n}$ is a function of population structure – in our model, weighted local density – but here integrated over an explicit competitive "neighborhood": $\tilde{n}(z,t) = \int_{z-h}^{z+h} \int_{L}^{U} xn(x,z,t)\,dx\,dz$ where h represents neighborhood size in the units of z. The demography-dispersal kernel $\tilde{K}$ is given by the sum of two parts, one that describes reproduction coupled with dispersal of propagules, and another that describes growth and survival of non-dispersing individu-

als:

$$\tilde{K}(x\prime, x, z\prime, z, \tilde{n}(z,t)) = K_{disp}(z\prime - z)Q(x\prime, x, \tilde{n}) + \delta(z\prime - z)G(x\prime, x, \tilde{n}) \tag{6}$$

Here, regeneration function Q and growth-survival function G correspond to Eq. 2, dispersal kernel K_{disp} corresponds to Eq. , and the Dirac delta function is a probability distribution with all mass at zero, which prevents movement. Following standard assumptions for integro-difference equations, we assume that space is one-dimensional and homogeneous, such that demographic transitions do not depend on location (or, more precisely, that they depend on location only through spatial variation in density) and the probability of dispersing from location z to $z\prime$ depends only on the absolute distance between them.

Under many conditions, models of this form generate traveling waves, and we are particularly interested in the velocity (m/yr) of this wave. Methods to estimate this velocity depend strongly on how demography responds to density. If fitness is maximized at some density $\tilde{n} > 0$ then the wave is pushed and wave velocity can only be estimated through numerical simulation. However, if fitness is maximized at $\tilde{n} = 0$ then the wave is pulled and an upper bound on its asymptotic velocity can be calculated analytically, following Neubert and Caswell (2000) and Jongejans et al. (2011), as

$$c^* = \min_{s>0} \left[\frac{1}{s} \ln(\rho_s) \right] \tag{7}$$

where s is a wave shape parameter and ρ_s is the dominant eigenvalue of the kernel $H_s(x\prime, x)$. Corresponding to Eq. 6 and assuming $\tilde{n} = 0$, H_s is composed of

$$H_s(x\prime, x) = M(s, x)Q(x\prime, x) + G(x\prime, x) \tag{8}$$

where $M(s, x)$ is the moment-generating function (MGF) for the dispersal kernel associated with size x. This formulation of the model assumes that the dispersal kernel depends only on maternal size x and not offspring size $x\prime$. To estimate $M(s, x)$ we simulated $N = 10000$ dispersal events (r) for each size x and marginalized these over one spatial dimension as in Lewis et al. (2006). We then evaluated the empirical MGF for each size x: $M(s) = \frac{1}{N} \sum_{i=1}^{N} e^{sr}$.

Estimates of wavespeed were bootstrapped for a total of 1000 replicates. Each bootstrap replicate recreated size- and density-dependent demographic models using 50% resampling on the original demographic data, and recreated dispersal kernels also using 50% resampling on the wind speeds and seed terminal velocities. Model selection for demographic vital rates was re-run for each bootstrap replicate. The empirical MGF relied on numerical sampling and was therefore sensitive to extreme long-distance events that differed across bootstrap realizations. Therefore, the distribution of bootstrapped wavespeeds reflects the combination of model uncertainty, parameter uncertainty, and stochasticity inherent to empirical MGFs.

Encroachment re-surveys

Finally, we used re-survey data from permanent transects to assess the predictions of the SIPM with respect to independent empirical observations. In summer 2001, shrub percent cover was recorded along two permanent 1000-m transects that spanned the shrub-grass ecotone (these were different transects than those described above for shrub demography). Surveys were conduced again in summer 2013 to document change in creosotebush abundance and spatial extent. At every 10 meters, shrub cover was recorded in nine cover classes (<1%, 1–4%, 5–10%, 10–25%, 25–33%, 33–50%, 50–75%, 75–95%, >95%). For visualization, we show midpoint values of these cover classes at each meter

location for both transects and years.

Results

Size and density dependent demography

Demographic data from naturally occurring and transplanted individuals revealed strong size- and density-dependence in demographic vital rates. For most sizes and vital rates, local density had negative demographic effects. Statistical support for size- and density-dependence is provided in Table XX, which provides AIC rankings for candidate models based on the completed (not bootstrapped) data set.

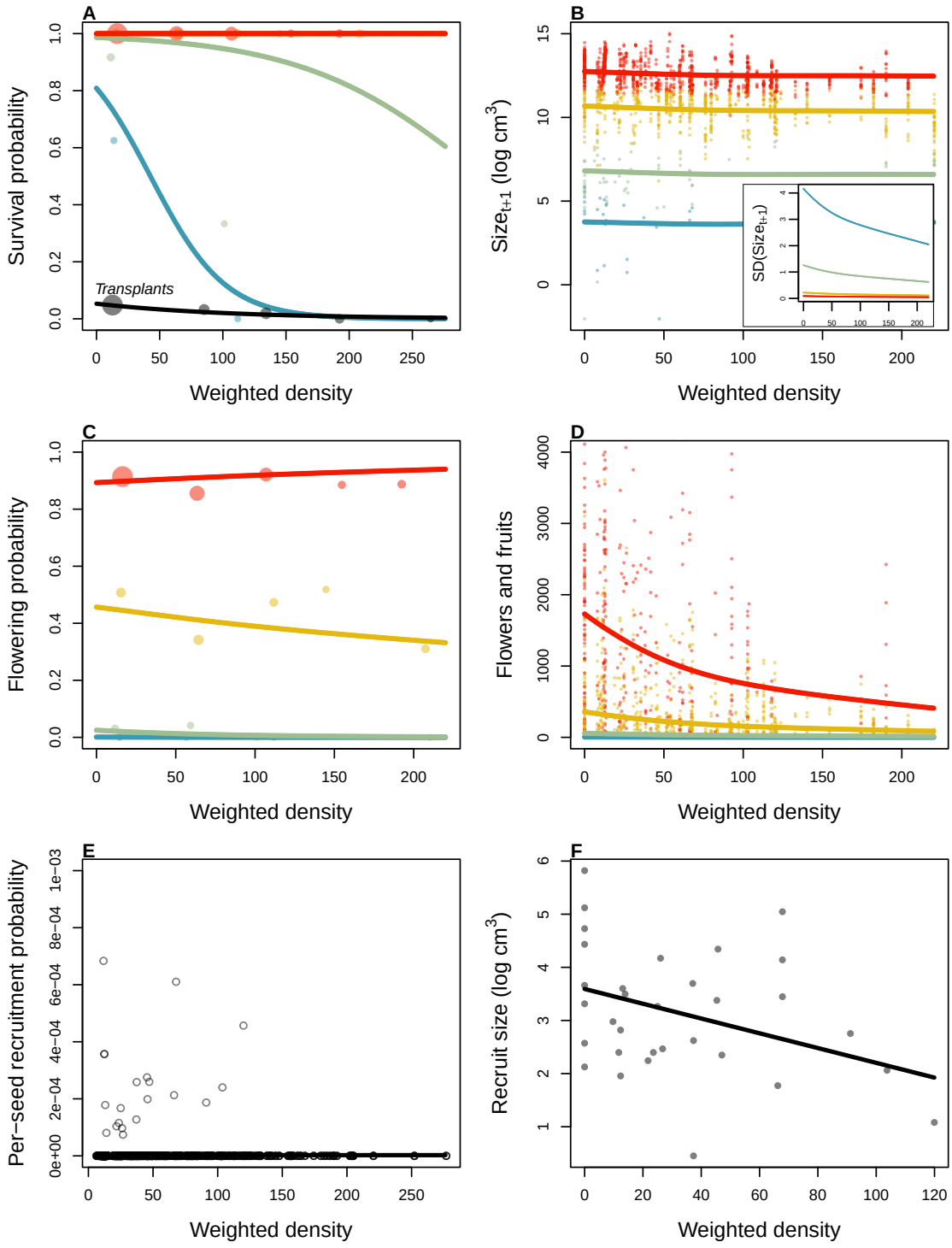

Figure 2: Size- and density-dependence in demographic vital rates. **A** Probability of survival from natural population census and transplant experiment (black line), **B** Mean and variance (inset) of size conditional on previous size, **C** Probability of flowering, **D** Flower and fruit production, **E** Probability of recruitment per seed, **F** Recruit size. In **A**–**E**, colored lines indicate four size groups (red is largest, blue is smallest), discretized for data visualization only. In all panels, weighted density is the sum of all plant sizes $log(cm^3)$ within the same 5-m window as the census individual.

Survival. Among naturally occurring plants, survival of large, established individuals was very high (Fig. 2A). We observed relatively few mortality events and nearly all of these were among new recruits. The probability of survival at these small sizes declined with increasing density. Survival of transplants was very low, lower even than survival of similarly-sized, naturally occurring recruits (Fig. 2B). However, the transplant results support the general pattern of negative density dependence in survival. Among the 20 survivors, 15 of them occurred in transect windows below the median of weighted shrub density.

SHORT PARAGRAPH SUMMARIZING SMALLER-SCALE ANALYSIS IN APPENDIX.

Growth. Current size was strongly predictive of future size, as expected, and there was weak negative density dependence in mean future size conditioned on current size (Fig. 2C). However, there was a stronger signal of density dependence in the variance of future size (Fig. 2C, inset). Plants at low density exhibited greater variance in growth trajectories and this was especially true at the smallest sizes. Thus, large increases (and decreases) in the size of new recruits were most likely to occur under low-density conditions.

Flowering and fruit production. Flowering probability was strongly size-dependent and and very weakly sensitive to local density (Fig. 2D). However, fertility of flowering plants was strongly negative density dependent, with greatest flower and fruit production by the largest plants at the lowest densities, and vice versa (Fig. 2E).

Recruitment and recruit size. We observed 32 natural recruitment events along our transects during the study years and our estimate recruitment rate, given total expected seed production in each window preceding the recruitment year, was very low (2.47×10^{-6},

2F). While most recruitment events occurred at low density, this is also where most seed production was concentrated (Fig. 2E) and low-density windows were over-represented relative to high density. For these reasons we were more likely to observe recruiment events at low density. Controlling for sampling effort and seed production, the statistical models indicated that our data were most consistent with a constant, density-independent recruitment rate (Table XX). However, the mean size of new recruits declined significantly with local density (Fig. 2F).

Population growth rate. As expected based on the vital rate results, the asymptotic population growth rate λ declined monotonically with density (Fig. 3). This was true across all bootstrap replicates, indicating high certainty that shrub fitness is maximized at zero density and thus that the expansion wave is "pulled". Mean growth rate at low density was 3% per year, with bootstrap uncertainty spanning 1–6%. At high density in the core of the expansion wave, population growth rates approached $\lambda = 1$, indicating population stasis driven by near-perfect survival and extremely rare recruitment.

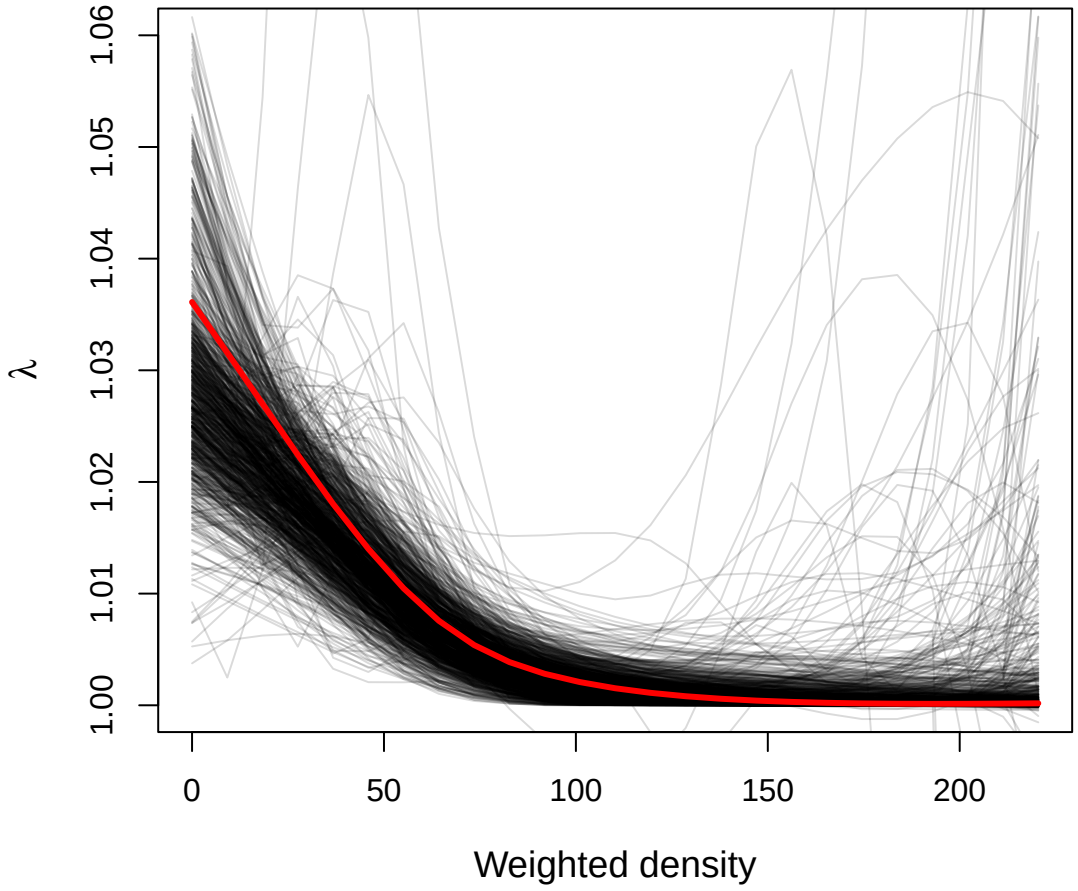

Figure 3: Density dependence in the asymptotic population growth rate (λ). Lines show bootstrap replicates sub-sampled from the full demographic data set. Weighted deighted density is the sum of all plant sizes $log(cm^3)$ within 5-m windows.

Seed dispersal

WALD dispersal kernels, inferred from the properties of seeds and wind and accounting for observed variation in wind speeds, were predicted to be strongly size dependent, with taller plants having a greater probability of dispersing seeds longer distances (Fig.

476 4). However, predicted seed dispersal was highly local, with most seeds expected to
477 fall within one meter of parent plants for most sizes. Even for the very tallest shrub
478 we observed (1.96 m), only 6.2% of its seeds were predicted to fall more than 3 m away
479 and less than 1% were predicted to fall more than 6 m away (Fig. 4). Taller shrubs also
480 exhibited wider variance in their dispersal kernel and this reflects their wider range of
481 seed release heights.

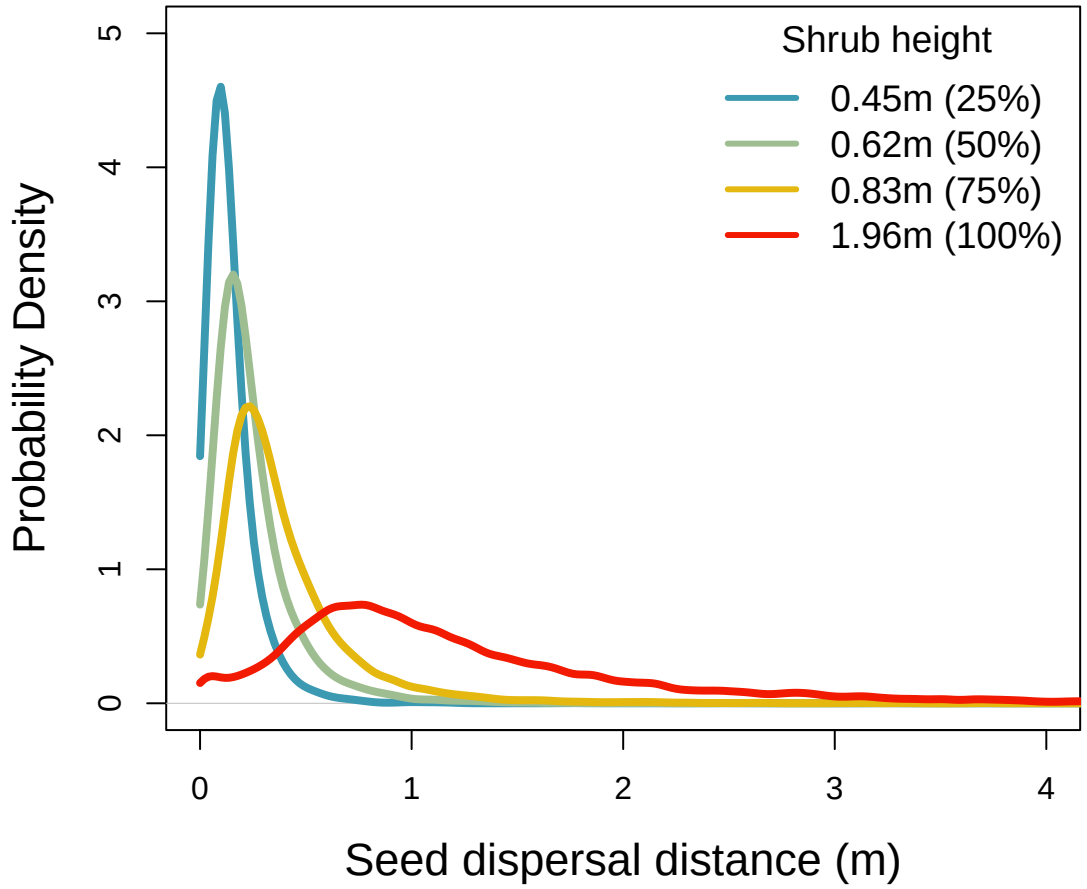

Figure 4: Predicted WALD dispersal kernels for four shrub heights corresponding to the 25th, 50th, 75th, and 100th (maximum) percentiles of the observed size distribution. We assume that heights below 15 cm have effectively no seed movement due to interference with the grass layer.

Expansion speed

The speed of encroachment at the study site as estimated by the SIPM is rather slow; as can be seen in Figure 5, the low-density wavefront moves at approximately 0.5 cm/yr under normal conditions and at 1 cm/yr under the best seedling survival conditions

observed in the dataset. These improved conditions were observed due to above-average rainfall that occurred after greenhouse-grown seedlings were transplanted to the site. Population growth in this low-density region of the moving wave is also low, with a geometric growth rate of $\lambda \approx 1.006$ and even lower rates of growth the higher-density regions behind; in the higher-survival scenario the maximum rate increases to $\lambda \approx 1.013$, with growth still decreasing as density increases. For both scenarios, the decrease in population growth rate with increasing density was monotonic across the range of observed standardised densities, as is shown in Figure 5. This suggests that an Allee effect is likely not present in this population, as the highest rate of population growth is found at the lowest density vanguard of the encroaching population. Thus, the conditions necessary for equation 9 to be valid are satisfied, and these wavespeeds are applicable for a pulled-wave scenario in which no Allee effects are present.

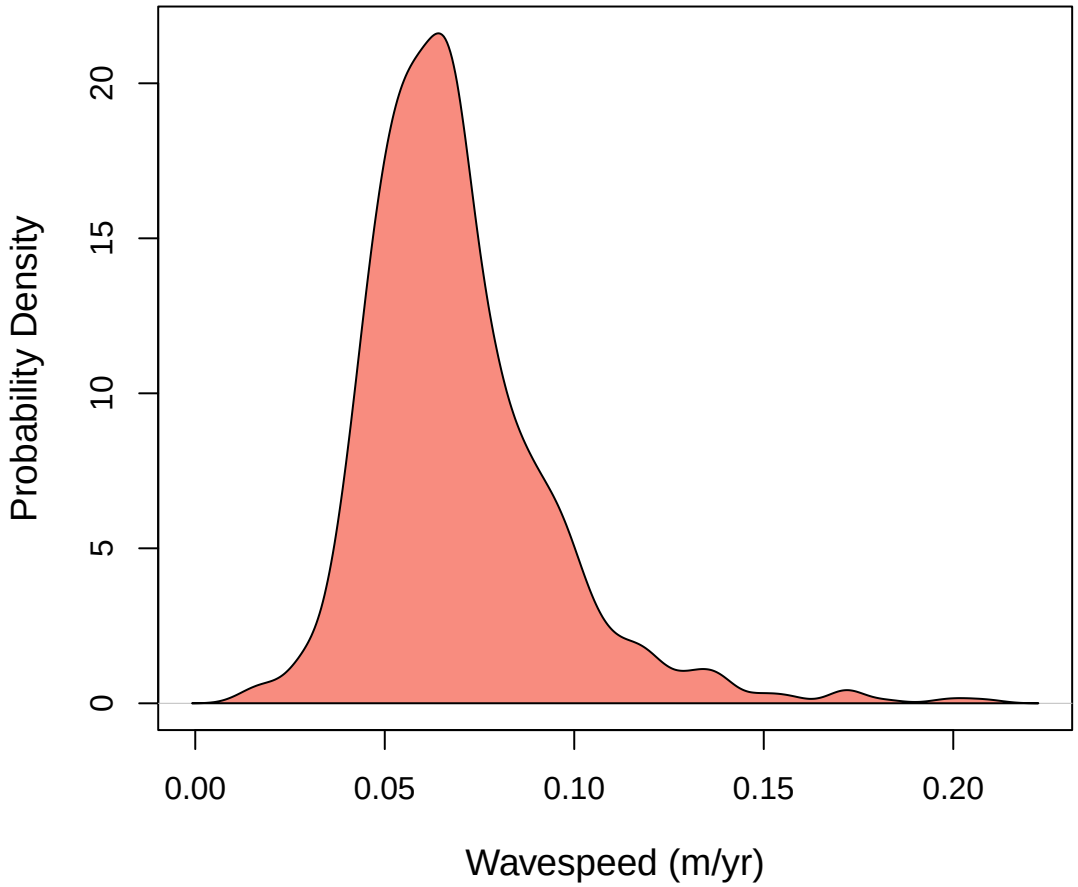

Figure 5: Estimated encroachment wave speeds (left) and geometric rates of population growth (right) for higher post-rainfall seedling survival and normal conditions.

Transect re-surveys

Re-surveys along two permanent transects revealed virtually no change the in the creosote expansion wave over 12 years . There were local changes in percent cover: on average cover increased by XX% between surveys. However, there was no clear indication that the leading edge of the creosote shrubland has advanced (the modest right-ward

shift on both transects is within the range of measurement error).

Discussion

The slow movement of the encroaching creosotebush wave at the Sevilleta LTER site can likely be contributed to a combination of three factors: short dispersal distances with extremely limited long-distance dispersal events, very low probability of recruitment from seed, and high seedling mortality. These three barriers, when combined, form a formidable challenge to the establishment of new shrubs at the low-density front of the wave. First, a seed must travel far enough to avoid competition with the parent shrub, which is unlikely given the dispersal kernels shown in Figure 2. Even if the seed manages to be dispersed this far, its chances of becoming a seedling are low. Caching and consumption by seed-eaters such as a variety of seed-harvesting ants (Lei, 1999; Whitford et al., 1980; Whitford, 1978) and the kangaroo rat Dipodomys merriami (Chew and Chew, 1970) decreases the amount of seeds available for germination. However, reduction in germination caused by destruction of seeds may be partly mitigated by the more favourable germination conditions that these seeds can experience when cached underground (Chew and Chew, 1970). Many of the remaining seeds will still fail to germinate, and in the unlikely event that germination does occur, seedlings will likely die given the high rates of mortality observed in smaller shrubs. Such high rates of creosotebush seedling mortality have been observed in other studies as well (Bowers et al., 2004; Boyd and Brum, 1983), probably due to a combination of herbivory, competition, and abiotic stresses.

However, as low as they are, the wavespeed estimates given in this paper are still conservative estimates for reasons mostly related to dispersal. First, it is important to note that the dispersal kernels used here, while they account for variation in factors

such as wind speed and terminal velocity, may underestimate the distances that shrub propagules travel. Because the WALD model assumes that terminal velocity is reached immediately upon seed release, seeds in the estimate thus take a shorter time to fall and have less time to be transported by wind, and the true frequency of long-distance dispersal events may thus be greater than what is estimated here. Second, dispersal at the study site could occur through additional mechanisms other than wind. For example, secondary dispersal through runoff from significant rainfall events can transport seeds (Thompson et al., 2014), and given that long-distance dispersal by bird and subsequent species divergence is thought to be responsible for creosotebush being in North America in the first place (Wells and Hunziker, 1976), short-distance dispersal by other animals at the study site likely occurs. As mentioned above, seeds are transported by seed-harvesting ants and granivorous mammals, where they are often stored in caches that can be appreciable distances from the parent shrubs. Whether transportation occurs via ant or rodent, creosotebush seeds can be moved significantly further than wind alone can, though many of these seeds are eventually consumed.

Despite the more conservative estimates our model yields, the estimated rate of dispersal in creosotebush populations at the Sevilleta National Wildlife Refuge is consistent with observations from the past 50-60 years, as creosotebush expansion during this time has been minimal (Moreno-de las Heras et al., 2016). However, it cannot explain the long-term increases in creosotebush cover at the study site, as total encroachment over the past 150 years is much greater than what would be expected given the encroachment rates derived by our models. Such a discrepancy is likely due to much of the expansion occurring in an episodic fashion, with short times during which rapid encroachment occurs due to favourable environmental conditions. This could be due in part to seedling recruitment, which is a factor that strongly limits creosotebush expansion, being rare

and episodic. For example, Allen et al. (2008) estimate that a major recruitment event occurred at this site in the 1950s, which is supported by photographic evidence from Milne et al. (2003) of a drought-driven expansion during this time. Moreno-de las Heras et al. (2016) estimate that after this expansion, several smaller creosotebush recruitment events occurred in decadal episodes. However, such events can be highly localised and may not necessarily occur at the low-density front of encroachment, which could explain how these recruitment events can still coexist with lack of encroachment in the recent past.

Overall, our observations and model highlight three aspects of creosotebush encroachment that should be the focus of future studies seeking to obtain better estimates of encroachment rates. First, negative density dependence in survival, growth, and reproduction is demonstrated, along with size dependence. The clear dependence on size and conspecific density suggests that they both should be considered when estimating creosotebush expansion and quantifying the demographic variation that contributes to it. Second, wind dispersal in these shrubs is quite limited; though the dispersal kernels seen here are typical in the sense that they are characterised by high near-plant dispersal and exceptionally low long-distance dispersal, the scale across which such dispersal occurs is small, with most seeds landing within only 1 m of the shrub. Wind dispersal alone may be an underestimate of the true amount of dispersal occurring, and future work should seek to incorporate the effects of dispersal by runoff and animals so that a more representative model of total dispersal can be obtained. Finally, encroachment is slow or even stagnates, but only most of the time. Though our encroachment speed estimates are representative of creosotebush populations for most years, the significant expansion seen over larger time scales suggests that there is episodic expansion in other years; while our model is consistent with the recent stagnation in creosotebush encroachment at the

Sevilleta LTER site, a model that also includes interannual variability in factors such as survival and recruitment would be able to better account for instances of episodic population expansion that are characteristic of this location.

Acknowledgements

Author contributions

Data accessibility

Literature Cited

Allen, A., W. Pockman, C. Restrepo, and B. Milne. 2008. Allometry, growth and population regulation of the desert shrub Larrea tridentata. Functional Ecology pages 197–204.

Bowers, J. E., R. M. Turner, and T. L. Burgess. 2004. Temporal and spatial patterns in emergence and early survival of perennial plants in the Sonoran Desert. Plant Ecology **172**:107–119.

Boyd, R. S., and G. D. Brum. 1983. Postdispersal reproductive biology of a Mojave Desert population of Larrea tridentata (Zygophyllaceae). American Midland Naturalist pages 25–36.

Brandt, J. S., M. A. Haynes, T. Kuemmerle, D. M. Waller, and V. C. Radeloff. 2013. Regime shift on the roof of the world: Alpine meadows converting to shrublands in the southern Himalayas. Biological Conservation **158**:116–127.

Buffington, L. C., and C. H. Herbel. 1965. Vegetational changes on a semidesert grassland range from 1858 to 1963. Ecological monographs **35**:139–164.

Bullock, J. M., S. M. White, C. Prudhomme, C. Tansey, R. Perea, and D. A. Hooftman. 2012. Modelling spread of British wind-dispersed plants under future wind speeds in a changing climate. Journal of Ecology **100**:104–115.

Cabral, A., J. De Miguel, A. Rescia, M. Schmitz, and F. Pineda. 2003. Shrub encroachment in Argentinean savannas. Journal of Vegetation Science **14**:145–152.

Chew, R. M., and A. E. Chew. 1970. Energy relationships of the mammals of a desert shrub (Larrea tridentata) community. Ecological Monographs pages 2–21.

D'Odorico, P., J. D. Fuentes, W. T. Pockman, S. L. Collins, Y. He, J. S. Medeiros, S. DeWekker, and M. E. Litvak. 2010. Positive feedback between microclimate and shrub encroachment in the northern Chihuahuan desert. Ecosphere **1**:1–11.

D'Odorico, P., G. S. Okin, and B. T. Bestelmeyer. 2012. A synthetic review of feedbacks and drivers of shrub encroachment in arid grasslands. Ecohydrology **5**:520–530.

Gandhi, S. R., E. A. Yurtsev, K. S. Korolev, and J. Gore. 2016. Range expansions transition from pulled to pushed waves as growth becomes more cooperative in an experimental microbial population. Proceedings of the National Academy of Sciences **113**:6922–6927.

Gardner, J. L. 1951. Vegetation of the creosotebush area of the Rio Grande Valley in New Mexico. Ecological Monographs **21**:379–403.

Gibbens, R., R. McNeely, K. Havstad, R. Beck, and B. Nolen. 2005. Vegetation changes in the Jornada Basin from 1858 to 1998. Journal of Arid Environments **61**:651–668.

Goslee, S., K. Havstad, D. Peters, A. Rango, and W. Schlesinger. 2003. High-resolution images reveal rate and pattern of shrub encroachment over six decades in New Mexico, USA. Journal of Arid Environments **54**:755–767.

Grover, H. D., and H. B. Musick. 1990. Shrubland encroachment in southern New Mexico, USA: an analysis of desertification processes in the American Southwest. Climatic change **17**:305–330.

Hsieh, C.-I., and G. G. Katul. 1997. Dissipation methods, Taylor's hypothesis, and stability correction functions in the atmospheric surface layer. Journal of Geophysical Research: Atmospheres **102**:16391–16405.

Huang, H., L. D. Anderegg, T. E. Dawson, S. Mote, and P. D'Odorico. 2020. Critical transition to woody plant dominance through microclimate feedbacks in North American coastal ecosystems. Ecology **101**:e03107.

Jongejans, E., K. Shea, O. Skarpaas, D. Kelly, and S. P. Ellner. 2011. Importance of individual and environmental variation for invasive species spread: a spatial integral projection model. Ecology **92**:86–97.

Katul, G., A. Porporato, R. Nathan, M. Siqueira, M. Soons, D. Poggi, H. Horn, and S. A. Levin. 2005. Mechanistic analytical models for long-distance seed dispersal by wind. The American Naturalist **166**:368–381.

Keitt, T. H., M. A. Lewis, and R. D. Holt. 2001. Allee effects, invasion pinning, and species' borders. The American Naturalist **157**:203–216.

Kelleway, J. J., K. Cavanaugh, K. Rogers, I. C. Feller, E. Ens, C. Doughty, and N. Saintilan. 2017. Review of the ecosystem service implications of mangrove encroachment into salt marshes. Global Change Biology **23**:3967–3983.

640 Knapp, A. K., J. M. Briggs, S. L. Collins, S. R. Archer, M. S. BRET-HARTE, B. E. Ewers,
641 D. P. Peters, D. R. Young, G. R. Shaver, E. Pendall, et al. 2008. Shrub encroachment in
642 North American grasslands: shifts in growth form dominance rapidly alters control of
643 ecosystem carbon inputs. Global Change Biology **14**:615–623.

644 Kot, M., M. A. Lewis, and P. van den Driessche. 1996. Dispersal data and the spread of
645 invading organisms. Ecology **77**:2027–2042.

646 Lei, S. A. 1999. Ecological impacts of Pogonomyrmex on woody vegetation of a Larrea-
647 Ambrosia shrubland. The Great Basin Naturalist pages 281–284.

648 Lewis, M., and P. Kareiva. 1993. Allee dynamics and the spread of invading organisms.
649 Theoretical Population Biology **43**:141–158.

650 Lewis, M. A., M. G. Neubert, H. Caswell, J. S. Clark, and K. Shea, 2006. A guide to cal-
651 culating discrete-time invasion rates from data. Pages 169–192 *in* Conceptual ecology
652 and invasion biology: reciprocal approaches to nature. Springer.

653 Mabry, T. J., J. H. Hunziker, D. Difeo Jr, et al. 1978. Creosote bush: biology and chemistry
654 of Larrea in New World deserts. Dowden, Hutchinson & Ross, Inc.

655 Maddox, J. C., and S. Carlquist. 1985. Wind dispersal in Californian desert plants:
656 experimental studies and conceptual considerations. Aliso: A Journal of Systematic
657 and Evolutionary Botany **11**:77–96.

658 Milne, B. T., D. I. Moore, J. L. Betancourt, J. A. Parks, T. W. Swetnam, R. R. Parmenter,
659 and W. T. Pockman. 2003. Multidecadal drought cycles in south-central New Mexico:
660 Patterns and consequences. Oxford University Press: New York, NY.

661 Moore, D., and K. Hall, 2022. Meteorology Data from the Sevilleta Na-

tional Wildlife Refuge, New Mexico. Environmental Data Initiative. https://doi.org/10.6073/pasta/d56307b398e28137dabaa6994f0f5f92.

Moreno-de las Heras, M., L. Turnbull, and J. Wainwright. 2016. Seed-bank structure and plant-recruitment conditions regulate the dynamics of a grassland-shrubland Chihuahuan ecotone. Ecology **97**:2303–2318.

Mugasi, S., E. Sabiiti, and B. Tayebwa. 2000. The economic implications of bush encroachment on livestock farming in rangelands of Uganda. African Journal of Range and Forage Science **17**:64–69.

Nathan, R., G. G. Katul, G. Bohrer, A. Kuparinen, M. B. Soons, S. E. Thompson, A. Trakhtenbrot, and H. S. Horn. 2011. Mechanistic models of seed dispersal by wind. Theoretical Ecology **4**:113–132.

Neubert, M. G., and H. Caswell. 2000. Demography and dispersal: calculation and sensitivity analysis of invasion speed for structured populations. Ecology **81**:1613–1628.

Oba, G., E. Post, P. Syvertsen, and N. Stenseth. 2000. Bush cover and range condition assessments in relation to landscape and grazing in southern Ethiopia. Landscape ecology **15**:535–546.

Pan, S., and G. Lin. 2012. Invasion traveling wave solutions of a competitive system with dispersal. Boundary Value Problems **2012**:120.

Parizek, B., C. M. Rostagno, and R. Sottini. 2002. Soil erosion as affected by shrub encroachment in northeastern Patagonia. Rangeland Ecology & Management/Journal of Range Management Archives **55**:43–48.

684 Peters, D. P., and J. Yao. 2012. Long-term experimental loss of foundation species:
685 consequences for dynamics at ecotones across heterogeneous landscapes. Ecosphere
686 **3**:1–23.

687 Ratajczak, Z., J. B. Nippert, and S. L. Collins. 2012. Woody encroachment decreases
688 diversity across North American grasslands and savannas. Ecology **93**:697–703.

689 Raupach, M. 1994. Simplified expressions for vegetation roughness length and zero-
690 plane displacement as functions of canopy height and area index. Boundary-Layer
691 Meteorology **71**:211–216.

692 Ravi, S., P. D'Odorico, S. L. Collins, and T. E. Huxman. 2009. Can biological invasions
693 induce desertification? The New Phytologist **181**:512–515.

694 Reed, M., L. Stringer, A. Dougill, J. Perkins, J. Atlhopheng, K. Mulale, and N. Favretto.
695 2015. Reorienting land degradation towards sustainable land management: Linking
696 sustainable livelihoods with ecosystem services in rangeland systems. Journal of envi-
697 ronmental management **151**:472–485.

698 Reynolds, J. F., R. A. Virginia, P. R. Kemp, A. G. De Soyza, and D. C. Tremmel. 1999.
699 Impact of drought on desert shrubs: effects of seasonality and degree of resource
700 island development. Ecological Monographs **69**:69–106.

701 Roques, K., T. O'connor, and A. R. Watkinson. 2001. Dynamics of shrub encroachment in
702 an African savanna: relative influences of fire, herbivory, rainfall and density depen-
703 dence. Journal of Applied Ecology **38**:268–280.

704 Schlesinger, W. H., and A. M. Pilmanis. 1998. Plant-soil interactions in deserts. Biogeo-
705 chemistry **42**:169–187.

706 Schlesinger, W. H., J. A. Raikes, A. E. Hartley, and A. F. Cross. 1996. On the spatial
707 pattern of soil nutrients in desert ecosystems: ecological archives E077-002. Ecology
708 **77**:364–374.

709 Schlesinger, W. H., J. F. Reynolds, G. L. Cunningham, L. F. Huenneke, W. M. Jarrell, R. A.
710 Virginia, and W. G. Whitford. 1990. Biological feedbacks in global desertification.
711 Science **247**:1043–1048.

712 Sirami, C., and A. Monadjem. 2012. Changes in bird communities in Swaziland savannas
713 between 1998 and 2008 owing to shrub encroachment. Diversity and Distributions
714 **18**:390–400.

715 Skarpaas, O., and K. Shea. 2007. Dispersal patterns, dispersal mechanisms, and invasion
716 wave speeds for invasive thistles. The American Naturalist **170**:421–430.

717 Sullivan, L. L., B. Li, T. E. Miller, M. G. Neubert, and A. K. Shaw. 2017. Density depen-
718 dence in demography and dispersal generates fluctuating invasion speeds. Proceed-
719 ings of the National Academy of Sciences **114**:5053–5058.

720 Taylor, C. M., and A. Hastings. 2005. Allee effects in biological invasions. Ecology Letters
721 **8**:895–908.

722 Thompson, S. E., S. Assouline, L. Chen, A. Trahktenbrot, T. Svoray, and G. G. Katul. 2014.
723 Secondary dispersal driven by overland flow in drylands: Review and mechanistic
724 model development. Movement ecology **2**:7.

725 Trollope, W., F. Hobson, J. Danckwerts, and J. Van Niekerk. 1989. Encroachment and
726 control of undesirable plants. Veld management in the Eastern Cape pages 73–89.

727 Turnbull, L., J. Wainwright, and R. E. Brazier. 2010. Changes in hydrology and erosion

over a transition from grassland to shrubland. Hydrological Processes: An International Journal **24**:393–414.

Van Auken, O. 2009. Causes and consequences of woody plant encroachment into western North American grasslands. Journal of environmental management **90**:2931–2942.

Van Auken, O. W. 2000. Shrub invasions of North American semiarid grasslands. Annual review of ecology and systematics **31**:197–215.

Vasek, F. C. 1980. Creosote bush: Long-lived clones in the Mojave Desert. American Journal of Botany **67**:246–255.

Veit, R. R., and M. A. Lewis. 1996. Dispersal, population growth, and the Allee effect: dynamics of the house finch invasion of eastern North America. The American Naturalist **148**:255–274.

Wang, M.-H., M. Kot, and M. G. Neubert. 2002. Integrodifference equations, Allee effects, and invasions. Journal of mathematical biology **44**:150–168.

Wells, P. V., and J. H. Hunziker. 1976. Origin of the creosote bush (Larrea) deserts of southwestern North America. Annals of the Missouri Botanical Garden pages 843–861.

Whitford, W., E. Depree, and P. Johnson. 1980. Foraging ecology of two chihuahuan desert ant species: Novomessor cockerelli andNovomessor albisetosus. Insectes Sociaux **27**:148–156.

Whitford, W. G. 1978. Structure and seasonal activity of Chihuahua desert ant communities. Insectes Sociaux **25**:79–88.

749 Wiernga, J. 1993. Representative roughness parameters for homogeneous terrain.
750 Boundary-Layer Meteorology **63**:323–363.

751 Williams, J. L., T. E. Miller, and S. P. Ellner. 2012. Avoiding unintentional eviction from
752 integral projection models. Ecology **93**:2008–2014.

753 Wood, S. 2017. Generalized Additive Models: An Introduction with R. 2 edition. Chap-
754 man and Hall/CRC.

Appendix A: Dispersal kernel modeling

WALD dispersal kernel. In order to create the dispersal kernel, we first take the wind speeds at measurement height z_m and correct them to find wind speed U for any height H by using the logarithmic wind profile [5]

$$U = \frac{1}{H} \int_{d+z_0}^{H} \frac{u^*}{K} \log\left(\frac{z-d}{z_0}\right) dz \tag{A1}$$

given in Bullock et al. (2012) equation 6, with the notation slightly modified. Here, z is the height above the ground, K is the von Karman constant, and u^* is the friction velocity. The zero-plane displacement d and roughness length z_0 are surface roughness parameters that, for a grass canopy height h above the ground, are approximated by $d \approx 0.7h$ and $z_0 \approx 0.1h$. These estimates are from Raupach (1994) for a canopy area index $\Lambda = 1$ in which the sum of grass canopy elements is equal to the unit area being measured. A 0.15 m grass height at our study site gives $d = 0.105$ and z_0, which are suitable approximations for grassland (Wiernga, 1993). Calculations of u^* were done using equation A2 from Skarpaas and Shea (2007), in which

$$u^* = KU_m \left[\log\left(\frac{z_m - d}{z_0}\right)\right]^{-1} \tag{A2}$$

and U_m is the mean wind velocity at the measurement height z_m. Values for the turbulent flow parameter σ were then calculated using the estimate made by Skarpaas and Shea (2007) in their equation A4, where

$$\sigma = 2A_w^2 \sqrt{\frac{K(z-d)u^*}{C_0 U}} \tag{A3}$$

[5] *We need to describe and cite the wind data used here.*

and C_0 is the Kolmogorov constant. A_w is a constant that relates vertical turbulence to friction velocity and is approximately equal to 1.3 under the assumptions of above-canopy flow made by Skarpaas and Shea (2007), based off calculations from Hsieh and Katul (1997). In addition, the assumption that $z = H$ was made in order to make the calculation of σ more feasible.[6]

The values from the previous three equations give us the necessary information to calculate μ' and λ', thus allowing us to create the WALD distribution $p(r)$. However, the base WALD model does not take into account variation in wind speeds or seed terminal velocities, which limits its applicability in systems where such variation is present. In order to account for this variation, we integrate the WALD model over distributions of these two variables using the same method as Skarpaas and Shea (2007). Additionally, the WALD model assumes seed release from a single point source, which is not realistic for creosote bush; because seeds are released across the entire height of the shrub rather than from a point source, we integrated $p(r)$ across the uniform distribution from the grass canopy height to the shrub height. Thus, under the assumptions that the height at which a seed is located does not affect its probability of being released and that seeds are evenly distributed throughout the shrub, this gives the dispersal kernel $K(r)$, where

$$K(r) = \iiint p(F)p(U)p(z)p(r)\,dF\,dU\,dz \tag{A4}$$

and $p(F)$ and $p(U)$ are the PDFs of the terminal velocity F and wind speed U, respectively, and $p(z)$ is the uniform distribution from h to H.

Dispersal data collection. The distribution $p(F)$ in the integral above was constructed using experimentally determined seed terminal velocities. This was done by using

[6] *Can you describe this assumption in biological terms?*

laboratory-based seed release experiments with a high-speed camera and motion tracking software to determine position as a function of time. We then used the Levenberg-Marquardt algorithm to solve a quadratic-drag equation of motion for F. Before seeds were released, they were dried, dyed with yellow fluorescent powder, and then put against a black background to improve visibility and make tracking easier. While the powder added mass to the seeds, this added mass only yielded an approximately 2.5% increase, likely having little effect on terminal velocities. Measurements were conducted for 48 seeds that were randomly chosen from a seed pool derived from different plants, and then an empirical PDF of terminal velocities was constructed using the data. Constructing $p(U)$ involved creating an empirical PDF of hourly wind speeds using data from Sevilleta LTER meterological station 49, the station closest to our transects. We used wind speed data collected hourly from 2015 to 2019 (Moore and Hall, 2022).

Appendix B: Model selection results

```
## Error in `[.data.frame`(aic_tables$surv_aic_out, , c("surv", "df", "dAIC")):
undefined columns selected
## Error in align(surv_aic) <- "c|p{12cm}|c|c|":  object 'surv_aic' not found
## Error in print(surv_aic, include.rownames = F, include.colnames = T, floating
= TRUE, :  object 'surv_aic' not found
```

mean(size)	sd(size)	df	dAIC
~size + (1|transect)	~1	3.00	1024.88
~size + density + (1|transect)	~1	8.50	977.23
~size + density + size:density + (1|transect)	~1	10.47	975.17
~size + (1|transect)	~size	9.65	146.23
~size + density + (1|transect)	~size	16.24	19.45
~size + density + size:density + (1|transect)	~size	18.55	19.62
~size + (1|transect)	~size + density	10.40	115.52
~size + density + (1|transect)	~size + density	18.97	0.08
~size + density + size:density + (1|transect)	~size + density	21.33	0.00

Table B1: AIC model selection for mean and variance of future size

Pr(Flowering)	df	dAIC
~size + (1|transect)	5.78	0.63
~size + density + (1|transect)	6.80	2.32
~size + density + size:density + (1|transect)	7.24	0.00

Table B2: AIC model selection for flowering probability.

No. fruits	df	dAIC
~size + (1|transect)	14.25	71.99
~size + density + (1|transect)	5.52	0.00
~size + density + size:density + (1|transect)	6.23	0.37

Table B3: AIC model selection for fruit number.

Pr(Recruitment)	df	dAIC
~(1|transect)	6.57	0.00
~density + (1|transect)	7.39	0.93

Table B4: AIC model selection for recruitment probability.

mean(size)	sd(size)	df	dAIC
~(1|transect)	~1	2.00	2.90
~density+(1|transect)	~1	4.42	0.00
~(1|transect)	~density	3.00	4.74
~density+(1|transect)	~density	5.56	1.21

Table B5: AIC model selection for mean and variance of recruit size.